

Synthesis of Ag–Pd Alloy Nanoparticles Suitable as Precursors for Ionic Migration-Resistant Conductive Film

Mari Yamamoto,[1] Hiroshi Kakiuchi,[2] Yukiyasu Kashiwagi,[1] Yukio Yoshida,[2] Toshinobu Ohno,[1] and Masami Nakamoto*[1]

[1]Osaka Municipal Technical Research Institute, 6-50, 1-Chome, Morinomiya, Joto-ku, Osaka 536-8553

[2]Daiken Chemical Co., LTD., 7-19, 2-Chome, Hanaten-nishi, Joto-ku, Osaka 536-0011

Received April 20, 2010; E-mail: nakamoto@omtri.or.jp

Tetradecanoate-stabilized Ag–Pd alloy nanoparticles (NPs) were quantitatively synthesized by the controlled thermolysis of silver tetradecanoate and palladium tetradecanoate in the presence of tripropylamine. This approach is a one-pot synthetic method applicable to large-scale preparation. The Ag–Pd alloy NPs obtained at feeding ratios of Ag/Pd = 85/15, 50/50, and 15/85 have mean diameters of about 3 nm with narrow size distributions. The structure of Ag–Pd alloy NPs was solid solution face-centered cubic (fcc) crystalline structure, which was confirmed by high-resolution transmission electron microscopy (HR-TEM) and powder X-ray diffraction (PXRD) measurement. The elemental compositions of the Ag–Pd alloy NPs corresponded closely with the feeding ratio of the precursors. The Ag–Pd alloy NPs were studied as printable precursors to fabricate conductive elements for printed electronics. The electronic circuit pattern was prepared by screen-printing, using Ag–Pd alloy NPs ink, and then converted to conductive film by annealing at 300 °C. The obtained metallic Ag–Pd alloy film had both high conductivity and ionic migration-resistance.

Metal nanoparticles (NPs) have unusual physical and chemical properties, quite different from those of larger particles, due to their smaller size and larger specific surface area.[1,2] Therefore, they are expected to have many potential applications in electronics, sensing, magnetics, optics, and catalysis.[3,4] One attractive application is printed electronics using ink containing metal NPs. It is of great interest as they become potentially low-cost materials for preparing large-area conductive film alternative to physically formed materials. In general, metal NPs with organic stabilizer are well dispersed in organic solvent. In addition, naked metal NPs without stabilizer in the extreme nanometer regime (<10 nm) melt at lower temperature. Because of this, the removal of the stabilizers by annealing may cause coalescence of the metal NPs, affording conductive film. Some examples have been reported of the use of Ag NPs as a precursor for conductive film, due to high conductivity.[5,6] Therefore, metal NPs can be applied to prepare inks with high metal concentration for printed electronics.

Recently, the demand for smaller devices has led to the reduction in spacing of wiring. Such fine pitch wiring causes problems with short circuits due to Ag ionic migration especially under conditions of high humidity. To prevent the migration, Ag–Pd alloy films have been prepared from coprecipitated 1.6 μm Ag–Pd powder.[7] In this case, high annealing temperature (850 °C) was required to afford conductive film. If Ag–Pd alloy NPs can be applied to make conductive film, the formation of fine pitch circuits with ionic migration-resistance may be achieved under low annealing temperature, compared with the coprecipitated micrometer size Ag–Pd powder. Torigoe et al. have reported the preparation of bimetallic Ag–Pd NPs through the decomposition of bimetallic oxalate complex by UV irradiation.[8] In another report, bimetallic Ag–Pd NPs with grape-like shape and a size around 30 nm were obtained by the thermolysis of metal salts in the presence of sodium dodecyl sulfate.[9] These reports suggest a possibility to develop a synthetic method for Ag–Pd alloy NPs with desired compositions and smaller than 10 nm. In addition, Ag–Pd alloy NPs have not been studied as a candidate for fabricating conductive elements for printed electronics. Thus, it is worthy to investigate the thermal properties of Ag–Pd alloy NPs for further applications.

Herein, we selected alkanecarboxylates as stabilizers for Ag–Pd alloy NPs in order to introduce weak interaction between stabilizer and metal core. The small 3 nm tetradecanoate-stabilized Ag–Pd alloy NPs were synthesized by the controlled thermolysis of silver tetradecanoate and palladium tetradecanoate in the presence of tripropylamine under mild conditions. Furthermore, we demonstrate that tetradecanoate-stabilized Ag–Pd alloy NPs ink can make conductive film with ionic migration-resistance under low annealing temperature.

Experimental

Reagents and Apparatus. All chemicals and solvents were reagent grade, obtained commercially and used without further purification. Silver nitrate, $AgNO_3$; palladium acetate, $[Pd_3(OAc)_6]$ (OAc: acetate); *n*-tetradecanoic acid, (n-$C_{13}H_{27}COOH$); tripropylamine; acetone; toluene; and terpineol (mixture of isomers) were obtained from Nakalai Tesque, Inc.

^{1}H NMR spectra were recorded on a JEOL JNM-AL300 instrument at 300 MHz using chloroform-*d* as a solvent and tetramethylsilane as an internal standard. The gas chromatograph mass spectroscopy (GC/MS) spectra were taken using a pyrolizer PY-2020D for thermal extraction at 200 °C for 10 min and a Hewlett-Packard 6890 GC system equipped with an

Published on the web October 30, 2010; doi:10.1246/bcsj.20100117

HP 5973 mass selective detector. The transmission electron microscopy (TEM) studies were performed with a JEOL JEM-1200EX (100 kV) operated at magnifications of 100000 times. The high-resolution transmission electron microscopy (HR-TEM) images were taken on a Hitachi H-9000 (300 kV) operated at magnifications of 400000 times. Samples for TEM and HR-TEM were prepared by placing a dispersion liquid of NPs in toluene on carbon-coated copper grids (JEOL, 200 mesh), followed by naturally evaporating the solvent at room temperature. The average diameter of NPs, standard deviation, and particle size distribution were determined from more than 200 particles based on TEM images. UV–visible absorption spectra of NPs re-dispersed in toluene were recorded on a Shimadzu UV-3150C spectrophotometer. The spectra were collected over the range of 300–800 nm. Powder X-ray diffractions (PXRDs) were measured using a Rigaku RINT 2500 diffractometer (Cu Kα radiation) equipped with a monochrometer operating at 40 kV and 50 mA. X-ray photoelectron spectroscopy (XPS) measured on a Physical Electronics (PHI) model 5700 ESCA spectrometer equipped with a Mg source (Mg Kα energy of 1253.6 eV) using BN as the internal standard and narrow scan photoelectron spectra were recorded for Ag($3d_{5/2}$) and Pd($3d_{5/2}$). The elemental compositions of the Ag–Pd alloy NPs were determined by XPS without using a standard sample. Default sensitivity coefficients of a PC-ACCESS data treatment system of PHI ESCA 5700 and peak areas were used for calculation of the atomic concentration. The thermogravimetric and differential thermal analyses (TG/DTA) were measured with a Seiko Instruments SSC/5200 thermal analyzer or Shimadzu TAG-50/DTA-50. The measurements were carried out from room temperature to 1000 °C with a heating rate of 20 °C min^{-1} under air flow. The thickness of the annealed film on the glass substrate was measured using an Accretech Surfcom1400A. Resistance was measured by Hewlett-Packard E2377A multimeter. The volume resistivity of the conductive film pattern with a length of 50 cm and width of 0.1 cm was calculated via the following equation.

$$\text{Volume resistivity } (\Omega\,\text{cm}) = \frac{\text{Resistance } (\Omega) \times \text{Thickness (cm)} \times \text{Width (cm)}}{\text{Length (cm)}} \quad (1)$$

The scanning electron microscopy (SEM) images were taken on a JEOL JSM-5600 operated at magnifications of 5000 and 20000 times. The in situ microscopic observation of Ag ionic migration was performed with a Keyence digital microscope VH-5000 operated at magnifications of 175 times. The bias was applied by using an Advantest DC Voltage current source/monitor TR6143.

Syntheses of Precursors. Silver tetradecanoate, Ag(*n*-$C_{13}H_{27}COO$) was prepared according to previously reported procedures.[10–13] Palladium tetradecanoate, [Pd_3(*n*-$C_{13}H_{27}COO)_6$] was prepared by ligand exchange of palladium acetate and *n*-tetradecanoic acid, as follows. Palladium acetate (1.12 g, 5 mmol) and *n*-tetradecanoic acid (3.45 g, 15 mmol) were added to 30 mL of toluene in a round-bottom flask, following constant stirring for 20 h under ambient atmosphere. The resulting solution was evaporated under reduced pressure to remove toluene and resultant acetic acid. [Pd_3(*n*-$C_{13}H_{27}COO)_6$] was purified by recrystallization from *n*-hexane at 0 °C. [Pd_3(*n*-$C_{13}H_{27}COO)_6$] was isolated as an orange powder (1.33 g, 2.4 mmol, yield 48%). ^{1}H NMR (300 MHz, $CDCl_3$, Me_4Si): δ_H 0.88 (t, 3H, $J = 6.6$ Hz, CH_3), 1.07–1.32 (m, 20H, CH_2), 1.39 (tt, 2H, $J = 7.3$, 7.3 Hz, $CH_2CH_2CO_2$), 2.17 (t, 2H, $J = 7.2$ Hz, CH_2CO_2).

Syntheses of Ag–Pd Alloy NPs. Silver tetradecanoate, Ag(*n*-$C_{13}H_{27}COO$) (503 mg, 1.5 mmol), palladium tetradecanoate, [Pd_3(*n*-$C_{13}H_{27}COO)_6$] (842 mg, 0.5 mmol), and tripropylamine (2.85 mL, 15 mmol) were placed in a 50 mL flask equipped with a magnetic stirrer. The reaction mixture was heated slowly in an oil bath and kept at 100 °C for 1 h under nitrogen. The reaction mixture was cooled to room temperature, and then acetone (20 mL) was added to the solution. The produced black precipitates were collected by centrifugation at 2000 rpm for 5 min, and dried under vacuum. The Ag–Pd alloy NPs prepared from the feeding molar ratio of Ag/Pd = 50/50, abbreviated as Ag–Pd(50/50) NPs, were isolated as a black powder (404 mg, yield 100% calculated from the metal content, 78%, estimated by thermogravimetric analysis).

The synthesis of Ag–Pd alloy NPs, Ag–Pd(85/15) NPs, and Ag–Pd(15/85) NPs, was conducted in the same manner as described above, except for the feeding molar ratios, Ag/Pd = 85/15 and 15/85, respectively. To form electronic circuits as described below, the large-scale synthesis of Ag–Pd(85/15) NPs was carried out on a 90-fold scale described above.

Syntheses of Ag NPs and Pd NPs. Ag NPs were prepared by the thermolysis of silver tetradecanoate, Ag(*n*-$C_{13}H_{27}COO$) (45.2 g, 135 mmol), in the presence of tripropylamine (128 mL, 675 mmol) at 100 °C for 1 h under nitrogen.[11,12] Pd NPs were also prepared by using palladium tetradecanoate, [Pd_3(*n*-$C_{13}H_{27}COO)_6$] (842 mg, 0.5 mmol) and tripropylamine (1.43 mL, 7.5 mmol) under the same conditions described above.

Formation of Conductive Films and Estimation of Ag Ionic Migration. The Ag–Pd(85/15) NPs and the Ag NPs were kneaded with terpineol for making the Ag–Pd alloy NPs ink (metal concentration: 59 wt %) and the Ag NPs ink (metal concentration: 82 wt %), respectively. A couple of electrodes with 0.75 mm spacing were printed on alumina substrates by screen-printing, using the Ag–Pd alloy NPs ink and the Ag NPs ink, respectively. The printed patterns were annealed at 300 °C for 30 min in an electronic furnace under air atmosphere to afford the conductive electrodes. Referring to Japan Electronics Packaging and Circuit Association (JPCA) standards (JCPA-ET01-09), the Ag ionic migration of the obtained Ag and Ag–Pd alloy electrodes was investigated by water drop method, respectively (Figure S1, see Supporting Information). A drop of distilled water was placed to bridge a couple of the electrode gap. A DC bias of 3 V was applied between these electrodes to evaluate Ag ionic migration. The in situ microscopic observation confirmed the growth of a dark layer from the cathode due to Ag ionic migration (Figure S2, see Supporting Information). The rate of Ag ionic migration was estimated by measuring the dark layer growth time from the cathode reaching the anode.

Results and Discussion

Syntheses and Properties of Ag–Pd Alloy NPs. A series of Ag–Pd alloy NPs with various compositions were synthesized through the simple one-pot thermolysis of silver tetradecanoate and palladium tetradecanoate in the presence of

Table 1. Analytical Data of Ag–Pd Alloy NPs

Ag–Pd alloy NPs	Metal content/wt %[a)]	Isolated yield/%[b)]
Ag–Pd(85/15) NPs	67	100
Ag–Pd(50/50) NPs	78	100
Ag–Pd(15/85) NPs	68	99

a) The metal contents show the weight % of metal in the NPs, measured by TG analysis. b) The isolated yields were calculated by the weight and metal content of the isolated NPs.

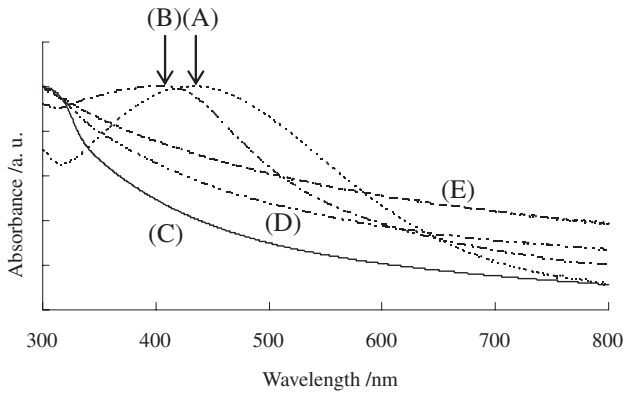

Figure 1. UV–vis absorption spectra of (A) Ag NPs, (B) Ag–Pd(85/15) NPs, (C) Ag–Pd(50/50) NPs, (D) Ag–Pd(15/85) NPs, and (E) Pd NPs.

tripropylamine. As the reaction mixture was heated from room temperature up to 100 °C, the light brown suspension gradually turned to dark brown around 60 °C, and then changed to black around 70 °C, resulting in a black solution at 100 °C. The reaction mixture was maintained at 100 °C for 1 h. After cooling to room temperature, acetone was added to precipitate the product. The product was collected by centrifugation and washed with acetone. A series of Ag–Pd alloy NPs were isolated as black powders in quantitative yield, as shown in Table 1. Even after prolonged storage of the Ag–Pd alloy NPs as powder in air, the Ag–Pd alloy NPs could be re-dispersed in common nonpolar organic solvents such as hexane and toluene by ultrasonication.

TG analysis indicates that the metal content in Ag–Pd(15/85) NPs was 68 wt %. The residual 32 wt % is the content of organic stabilizer. The metal contents in Ag–Pd alloy NPs determined by TG analysis are summarized in Table 1. The GC/MS analysis of Ag–Pd alloy NPs suggests the existence of tetradecanoic acid ($m/z = 228$) as organic stabilizer, but not tripropylamine. Thus, only the tetradecanoate attaches on the surface of the Ag–Pd core. This result corresponds to tetradecanoate-stabilized Ag NPs prepared by the same procedure.[11,12]

UV–vis absorption spectra of Ag–Pd alloy NPs with different compositions are shown in Figure 1, together with the Ag NPs and Pd NPs, respectively. The Ag NPs show strong surface plasmon resonance (SPR) centered at 432 nm (Figure 1A), while the Pd NPs do not show distinct absorption (Figure 1E). The broad absorption may be due to d–d interband transitions.[14–18] On the other hand, the SPR peak of the Ag–Pd(85/15) NPs becomes broader and shifts to lower wavelength, 405 nm in Figure 1B, compared with that of the Ag NPs. This phenomenon is consistent with a previously reported computer simulation of the composition dependence of plasma

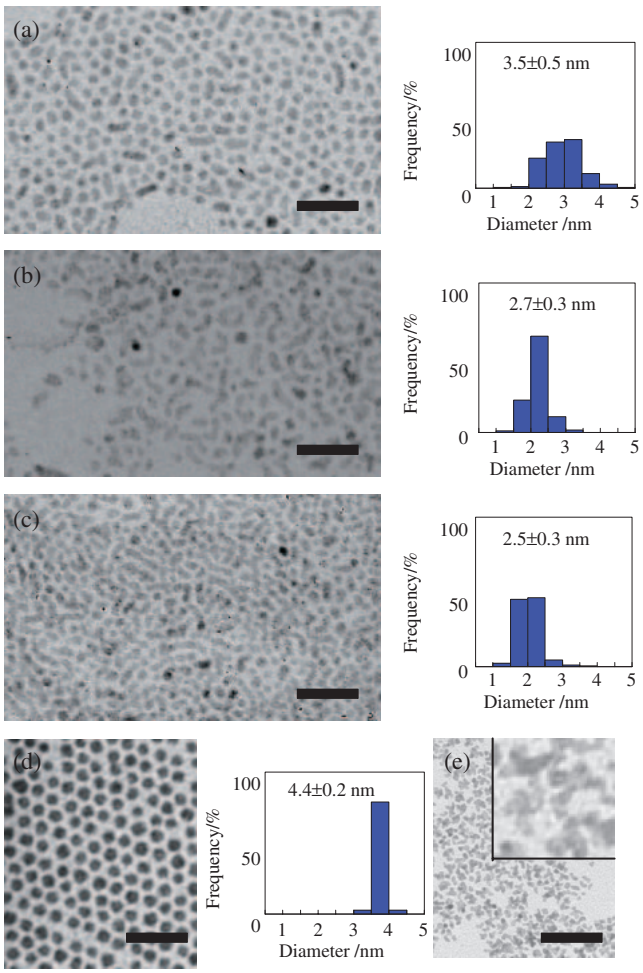

Figure 2. TEM images and the corresponding particle size distribution analyses of (a) Ag–Pd(85/15) NPs, (b) Ag–Pd(50/50) NPs, (c) Ag–Pd(15/85) NPs, (d) Ag NPs, and (e) Pd NPs (inset: multipods formed by coalescence of primary Pd NPs) (scale bar: 20 nm).

wavelength using bulk dielectric constants of Ag and Pd, together with a measurement of UV–vis absorption spectrum of Ag–Pd alloy nanoparticles.[8] Furthermore, the spectra of Ag–Pd(50/50) NPs and the Ag–Pd(15/85) NPs show no prominent absorption peaks (Figures 1C and 1D). It is known that the presence of a group 10 element (Pd) in the alloy NPs usually suppresses the SPR of a group 11 element (Ag).[19–22] Therefore, no distinct absorption peaks were observed. This suggests the formation of bimetallic nanoparticles. Similar spectra were also reported for Ag–Pt,[23] Au–Pd,[24] and Au–Pt[25] alloy NPs. The structure and elemental compositions of the Ag–Pd alloy NPs further investigated by HR-TEM, XRD, and XPS analysis are described below.

Particle Size Analysis of Ag–Pd Alloy NPs. The TEM images and size distributions of the Ag–Pd alloy NPs with different compositions are shown in Figures 2a–2c, together with those of the Ag NPs (Figure 2d) and the Pd NPs (Figure 2e), respectively. TEM samples were prepared by using toluene suspensions of the NPs directly without size selection. The primary particle size of Ag–Pd alloy NPs, Ag–Pd(85/15) NPs, Ag–Pd(50/50) NPs, and Ag–Pd(15/85)

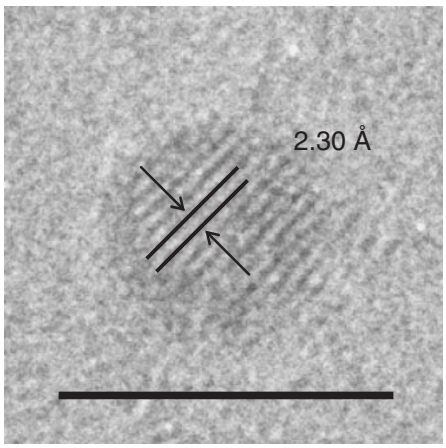

Figure 3. HR-TEM image of Ag–Pd(50/50) NPs. The measured average spacing of the fringes is 2.30 Å. (scale bar: 5 nm).

NPs, were 3.5 ± 0.5, 2.7 ± 0.3, and 2.5 ± 0.3 nm, respectively (Figures 2a–2c). The mean diameter of the Ag NPs was 4.4 ± 0.2 nm (Figure 2d). On the other hand, the shape of Pd NPs was multipod due to the coalescence of the primary particles (Figure 2e, inset). As the feeding molar ratio of Pd increased, the coalescence of the primary particles proceeded. It has been reported that ligands such as thiol[18] and thioether[26] with strong interaction to Pd afford spherical Pd NPs, while ligands such as amine with weak interaction with Pd induces the agglomeration of the primary particles.[27] In our case, the alkylcarboxylate ligands have weaker interaction with the more noble metal, Pd, rather than Ag. Thus, this weaker interaction of alkylcarboxylate ligand with Pd induces the coalescence of the primary particles.

Structure and Composition Analysis of Ag–Pd NPs. The structure of Ag–Pd(50/50) NPs was characterized in detail by HR-TEM as shown in Figure 3. The HR-TEM image of Ag–Pd(50/50) NPs displayed continuous fringes with the same orientation. It suggests that each Ag–Pd(50/50) NPs is a single crystal with alloy structure, but not core–shell or twin structure. The average fringe spacing with a period of 2.30 Å corresponds to the mean value between {111} lattice spacing of face centered cubic (*fcc*)-Ag (2.36 Å) and *fcc*-Pd (2.25 Å). This also suggests that the Ag–Pd(50/50) NPs have alloy structure. In addition, the average fringe spacing of several Ag–Pd(50/50) NPs corresponded with each other. This indicates that the elemental ratios of each Ag–Pd(50/50) NP were uniform.

The alloy structures of the Ag–Pd alloy NPs were also supported by PXRD. The PXRD patterns of Ag–Pd alloy NPs with various compositions are shown in Figures 4b–4d together with the Ag NPs (Figure 4a) and the Pd NPs (Figure 4e), respectively. PXRD patterns of the Ag–Pd alloy NPs show only one broad peak (Figures 4b–4d). The broad peak indicated the Ag–Pd alloy NPs were small crystallite as usually observed for NPs. The average crystallite sizes were calculated from the half value width of (111) reflection using Scherrer's equation.[28] The calculated crystallite sizes, 3.2–3.7 nm, of Ag–Pd alloy NPs were fairly consistent with those obtained from TEM images. The peak position of Ag–Pd alloy NPs was located between the (111) diffraction peak position of *fcc*-Ag ($2\theta = 38.3°$) observed

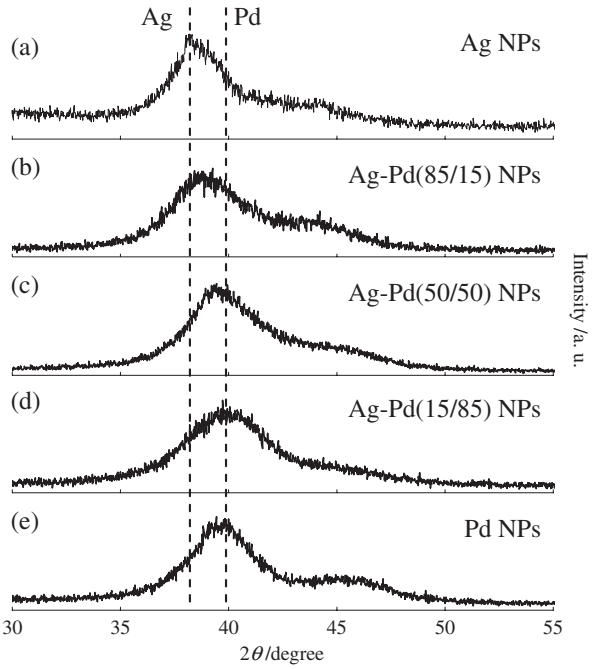

Figure 4. PXRD patterns of (a) Ag NPs, (b) Ag–Pd(85/15) NPs, (c) Ag–Pd(50/50) NPs, (d) Ag–Pd(15/85) NPs, and (e) Pd NPs.

Table 2. Quantitative XPS Analysis Data of Ag–Pd Alloy NPs

Ag–Pd alloy NPs	Feeding molar ratio Ag/Pd	Elemental molar ratio Ag/Pd on the surface of NPs[a)]
Ag–Pd(85/15) NPs	85/15	84/16
Ag–Pd(50/50) NPs	50/50	52/48
Ag–Pd(15/85) NPs	15/85	17/83

a) The elemental molar ratios of Ag/Pd were estimated based on peak areas of $Ag(3d_{5/2})$ and $Pd(3d_{5/2})$ and their default sensitivity coefficients.

for the Ag NPs and that of *fcc*-Pd ($2\theta = 39.4°$) observed for the Pd NPs. The (111) diffraction peak position of Ag–Pd alloy NPs continuously shifted toward higher 2θ angle with decreasing the Ag ratios. This phenomenon revealed that the interplaner spacing changed by the composition of each Ag–Pd alloy NPs. Therefore, these results suggested that the elemental compositions of Ag–Pd alloy NPs were proportional to the feeding molar ratios.

Table 2 shows the elemental molar ratios of Ag–Pd NPs examined by XPS analysis by using default sensitivity coefficients and peak areas. Considering the error range of elemental ratios determined by XPS analysis, the elemental ratios of Ag–Pd NPs largely corresponded to the feeding molar ratios. All of the precursors were completely consumed to become NPs, because the isolated yields were quantitative as shown in Table 1. In addition, according to the HR-TEM images, continuous fringes with the same orientation were observed. Therefore, the elemental compositions are almost the same from surface to center of Ag–Pd alloy NPs.

Formation of Conductive Film by the Use of Ag–Pd NPs Ink and Its Resistance to Ionic Migration. In a previous

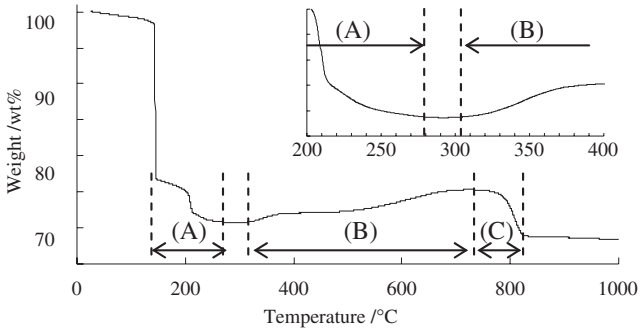

Figure 5. TG analysis of Ag–Pd(15/85) NPs. The ranges (A–C) show (A) the decomposition and removal of tetradecanoate ligand, (B) the oxidation of Pd, and (C) the decomposition of PdO, respectively (inset: magnified figure in the range from 200 to 400 °C).

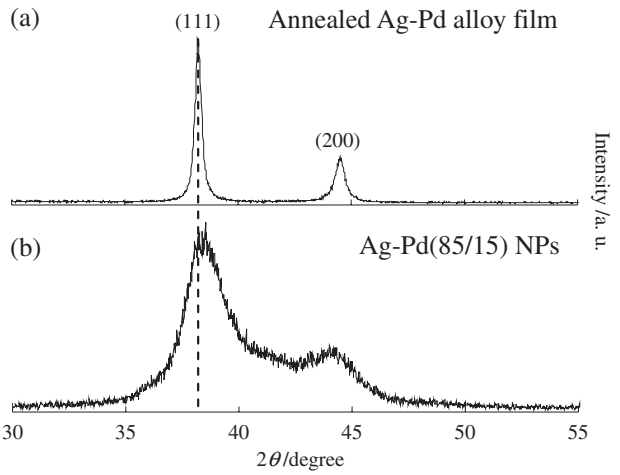

Figure 6. PXRD patterns of (a) the annealed Ag–Pd alloy film, using Ag–Pd(85/15) NPs ink, and (b) Ag–Pd(85/15) NPs.

report,[6] we demonstrated that alkanecarboxylate-stabilized Ag NPs could afford conductive film through the removal of stabilizer by annealing. Similar to the Ag NPs, we demonstrate the formation of conductive film by using tetradecanoate-stabilized Ag–Pd alloy NPs. In order to investigate the thermal behavior of the Ag–Pd alloy NPs, TG analysis was carried out from room temperature to 1000 °C with a heating rate of 20 °C min^{-1} under air. Figure 5 depicts the representative TG profile of Ag–Pd(15/85) NPs. The profile shows a sharp weight decrease at 143 °C and continuous weight decrease around 214 °C (range A) due to decomposition and evaporation of organic stabilizer on the surface of Ag–Pd alloy NPs. On the other hand, weight increase was observed over a wide temperature range from 320 to 730 °C (range B), but followed by decrease again from 730 to 821 °C (range C). In order to examine this, PXRD analysis was carried out for the Ag–Pd(15/85) NPs heated from room temperature to 400, 600, and 900 °C with a heating rate of 20 °C min^{-1} under air, respectively. (Figure S3, see Supporting Information) The Ag–Pd(15/85) NPs heated to 400 °C show a sharp diffraction peak corresponding to Ag–Pd(15/85) alloy phase, while heating to 600 °C gives rise to a PdO phase, together with Ag–Pd alloy phase. Heating to 900 °C shows a weak diffraction peak of PdO phase, together with a strong diffraction peak of Ag–Pd alloy phase. This indicates that the weight increase at range B is from partial oxidation of Pd in the alloy to PdO, and the weight decrease at range C shows the decomposition of the resulting PdO to Ag–Pd, respectively. The ratio of weight decrease at range C decreased from 36, 17, to 9 mol % as an oxygen atom in the order of Ag–Pd(15/85) NPs, Ag–Pd(50/50) NPs, and Ag–Pd(85/15) NPs, respectively. This also supports the proposition that a portion of Pd, instead of Ag, in the Ag–Pd alloy nanoparticles is oxidized.

According to the TG profile of Ag–Pd(85/15) NPs (Figure S4, see Supporting Information), tetradecanoate ligands were completely removed around 303 °C (range A), and then the oxidation of Pd started around 390 °C (range B). According to this, the annealing temperature of Ag–Pd(85/15) NPs was determined in the range from 300 to 390 °C. The Ag–Pd alloy conductive film was formed as follows. The Ag–Pd NPs ink was prepared by mixing Ag–Pd(85/15) NPs powder and terpineol as a solvent and electronic circuit patterns were prepared by screen printing. The printed Ag–Pd NPs electrode pattern was annealed in an electronic furnace at 300 °C for 30 min under air. Shiny black Ag–Pd alloy conductive film was obtained. The Ag–Pd alloy conductive film displayed smooth edges throughout the pattern and good uniformity with an average thickness of 2.1 μm. Figure 6 shows the PXRD pattern of the resulting conductive film together with the Ag–Pd(85/15) NPs. In spite of the annealing under atmospheric conditions, oxidation of Pd did not occur during film formation. The diffraction peak positions of the Ag–Pd alloy conductive film exactly coincided with that of the Ag–Pd(85/15) NPs. It indicates the conductive film maintains the Ag–Pd alloy structure. The average crystallite sizes calculated by Scherrer's equation[28] were 41.9 nm for the Ag–Pd alloy conductive film and 5.1 nm for Ag–Pd(85/15) NPs, respectively. It suggests that the size evolution from smaller to larger particles by heat-induced coalescence of NPs occurred during annealing. Figure 7 shows the SEM images of the surface and the cross section of the Ag–Pd alloy conductive film. The surface of the film shows uniform surface without visible signs of cracks (Figure 7a). The cross section of the film shows continuous contacts of larger coalesced particles of ≈500 nm (Figure 7b). The volume resistivity of the Ag–Pd alloy conductive film was 12.1 μΩ cm. It was close to that of bulk Ag (1.6 μΩ cm) and Pd (10.4 μΩ cm). This high conductivity is sufficient for application to electronic devices. The tetradecanoate ligand avoids the aggregation of the NPs as powder at room temperature and affords the dispersion liquid. But this stabilizer was easily removed from NPs at 300 °C to induce coalescence. This is of critical importance for affording conductive film.

Concerning the Ag ionic migration, the relative evaluation of Ag–Pd alloy electrode and Ag electrode was carried out by using water drop test, as shown in Figure S1 (see Supporting Information). A drop of deionized water was placed to bridge a couple of the electrode gap (electrode spacing: 0.75 mm). A DC 3 V bias was applied between these electrodes to evaluate Ag ionic migration. The in situ microscopic observation confirmed that the growth of the dark layer from the cathode reached to the anode, due to Ag ionic migration (Figure S2, see Support-

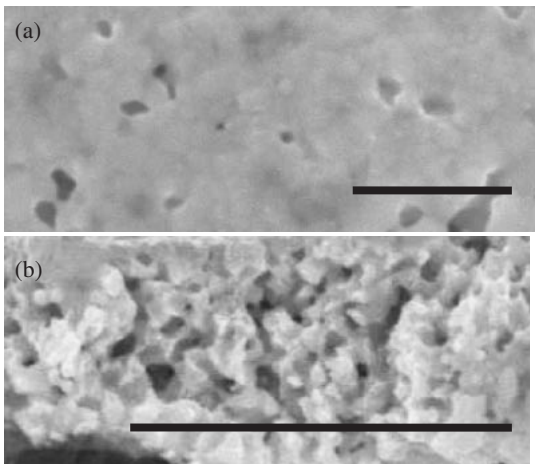

Figure 7. SEM images of (a) the surface (scale bar: 1 μm) and (b) the cross section (scale bar: 5 μm) of the annealed Ag–Pd alloy film.

ing Information). The formation time of the dark layer on the Ag–Pd alloy electrode was improved to be 555 s, quite different from that of Ag electrode, 157 s. Thus, the Ag–Pd alloy conductive film formed from the Ag–Pd alloy NPs ink was effective to reduce Ag ionic migration.

Conclusion

The large-scale synthesis of Ag–Pd alloy NPs with various compositions has been accomplished by controlled thermolysis of silver tetradecanoate and palladium tetradecanoate in the presence of tripropylamine. The elemental compositions of the Ag–Pd alloy NPs nearly corresponded to the feeding molar ratios. The HR-TEM and PXRD analyses suggest the formation of alloy structure. Thus, the NPs have the same composition from the surface to center of particles. These tetradecanoate-stabilized Ag–Pd alloy NPs were suitable as the precursor for printed electronics. The ink with high metal concentration (58 wt %) could be easily prepared by using Ag–Pd alloy NPs. The mild annealing of the printed Ag–Pd alloy NPs electrode pattern induced the removal of stabilizer and the coalescence of Ag–Pd alloy core. The volume resistivity of the resulting Ag–Pd alloy film was close to those of bulk silver and palladium. Compared with the Ag electrode, the Ag–Pd alloy electrode had the resistance to the ionic migration.

We thank Dr. Takao Sakata and Prof. Hirotaro Mori at the Research Center for Ultra-High Voltage Electron Microscopy, Osaka University for the assistance and discussions of HR-TEM measurements. This work was financially supported by Grant-in-Aid for Science Reasarch (No. 18710080) and also by Osaka Central Area Industry-Government-Academia Collaboration Project on "City Area Program," 2007–2009, from the Ministry of Education, Culture, Sports, Science and Technology, Japan, respectively.

Supporting Information

Sketch of the experiment by water drop method (Figure S1), microscopic images of ionic migration test (Figure S2), XRD patterns of heated Ag–Pd(15/85) NPs (Figure S3), and TG profile of Ag–Pd(85/15) NPs (Figure S4). This material is available free of charge on the web at http://www.csj.jp/journals/bcsj/.

References

1 *Nanoparticles: From Theory to Application*, 1st ed., ed. by G. Schmid, Wiley-VCH, Weinhein, **2004**.
2 *Nanoparticles and Nanostructured Films: Preparation, Characterization and Applications*, 1st ed., ed. by J. H. Fendler, Wiley-VCH, Weinhein, **1998**.
3 *Metal Nanoclusters in Catalysis and Materials Science: The Issue of Size Control*, 1st ed., ed. by B. Corain, G. Schmid, N. Toshima, Elsevier, Amsterdam, **2008**.
4 *Nanoparticle Technology Handbook*, 1st ed., ed. by M. Hosokawa, K. Nogi, M. Naito, T. Yokoyama, Elsevier, Amsterdam, **2007**.
5 Y. Li, Y. Wu, B. S. Ong, *J. Am. Chem. Soc.* **2005**, *127*, 3266.
6 M. Nakamoto, in *Nanoparticle Technology Handbook*, 1st ed., ed. by M. Hosokawa, K. Nogi, M. Naito, T. Yokoyama, Elsevier, Amsterdam, **2007**, Applications 4, pp. 434–438.
7 J.-C. Lin, J.-Y. Chuang, *J. Electrochem. Soc.* **1997**, *144*, 1652.
8 K. Torigoe, K. Esumi, *Langmuir* **1993**, *9*, 1664.
9 C.-C. Yang, C.-C. Wan, Y.-Y. Wang, *J. Colloid Interface Sci.* **2004**, *279*, 433.
10 K. Abe, T. Hanada, Y. Yoshida, N. Tanigaki, H. Takiguchi, H. Nagasawa, M. Nakamoto, T. Yamaguchi, K. Yase, *Thin Solid Films* **1998**, *327–329*, 524.
11 M. Yamamoto, M. Nakamoto, *J. Mater. Chem.* **2003**, *13*, 2064.
12 M. Yamamoto, Y. Kashiwagi, M. Nakamoto, *Langmuir* **2006**, *22*, 8581.
13 Y. Kashiwagi, M. Yamamoto, M. Nakamoto, *J. Colloid Interface Sci.* **2006**, *300*, 169.
14 X. Z. Lin, X. Teng, H. Yang, *Langmuir* **2003**, *19*, 10081.
15 A. Taleb, C. Petit, M. P. Pileni, *Chem. Mater.* **1997**, *9*, 950.
16 P. Mulvaney, *Langmuir* **1996**, *12*, 788.
17 J. A. Creighton, D. G. Eadon, *J. Chem. Soc., Faraday Trans.* **1991**, *87*, 3881.
18 S. Chen, K. Huang, J. A. Stearns, *Chem. Mater.* **2000**, *12*, 540.
19 M.-L. Wu, D.-H. Chen, T.-C. Huang, *Langmuir* **2001**, *17*, 3877.
20 N. Toshima, T. Yonezawa, *New J. Chem.* **1998**, *22*, 1179.
21 M. Harada, K. Asakura, N. Toshima, *J. Phys. Chem.* **1993**, *97*, 5103.
22 H. Liu, G. Mao, S. Meng, *J. Mol. Catal.* **1992**, *74*, 275.
23 S. Remita, M. Mostafavi, M. O. Delcourt, *Radiat. Phys. Chem.* **1996**, *47*, 275.
24 N. Toshima, M. Harada, Y. Yamazaki, K. Asakura, *J. Phys. Chem.* **1992**, *96*, 9927; X. Teng, Q. Wang, P. Liu, W. Han, A. I. Frenkel, W. Wen, N. Marinkovic, J. C. Hanson, J. A. Rodriguez, *J. Am. Chem. Soc.* **2008**, *130*, 1093.
25 N. Toshima, T. Yonezawa, *Makromol. Chem., Macromol. Symp.* **1992**, *59*, 281.
26 M. Ganesan, R. G. Freemantle, S. O. Obare, *Chem. Mater.* **2007**, *19*, 3464.
27 N. Kijima, Y. Takahashi, J. Akimoto, T. Tsunoda, K. Uchida, Y. Yoshimura, *Chem. Lett.* **2005**, *34*, 1658.
28 P. Scherrer, *Göttinger Nachr.* **1918**, *2*, 98; H. P. Klug, L. E. Alexander, *X-ray Diffraction Procedures*, 2nd ed., Wiley, New York, **1973**.